

AN EXPERIMENTAL AND NUMERICAL INVESTIGATION ON THE DIESEL AFTER-TREATMENT SYSTEMS

¹Wang, Tae Joong*, ¹Baek, Seung Wook, ²Lee, Je-Hyung
¹KAIST, Korea, ²Hyundai-Kia Motor, Korea

KEYWORDS – Diesel emission, after-treatment system, catalytic reaction, DOC, SCR

ABSTRACT - Related to the expansion of diesel share in the market, emission problem has become an indispensable obligation of the car makers. In this study, an experimental investigation of commercial DOC (diesel oxidation catalyst), which is designed to reduce the SOF of diesel PM as well as gaseous CO and HC, was performed through engine dynamometer tests, and its numerical modeling was accomplished using the data. In addition, SCR (selective catalytic reduction) system, which reduces diesel NO_x, was also modeled and integrated into the DOC. Thus, all kinds of diesel emissions except soot were completely monitored through the developed analytic tools. Based on the simulated results, optimum operating conditions and geometric configurations of diesel after-treatment systems were proposed.

TECHICAL PAPER – On modeling the catalytic converter system, the reaction kinetics is definitely one of the most critical factors to determine the accuracy. Particularly in catalytic reaction, the kinetics is quite arbitrary and has a case-by-case nature because it is affected by a lot of parameters related to the catalyst preparations. Therefore, the calibration procedure through an experimental work is needed for the establishment of an exact numerical model. In this study, based on our own experimental data, we developed numerical models on the commercial DOC and SCR systems. Also, with these tools, we simulated the DOC and SCR behaviors, and investigated the effects of various system parameters, such as catalyst temperature, space velocity, cell density, and catalyst loading, on the performance.

DOC EXPERIMENT

Engine-dynamometer experiments were conducted with mounting a DOC on the exhaust pipe line. Schematic view of the test cell set-up is illustrated in Fig. 1. For the experiment, a 2.0 liter diesel engine and a commercial round-type 400 cpsi DOC were used. The engine was connected to a 160kW EC dynamometer controlled with the PUMA 5.3 system. A test cell computer controls engine speed and load, as well as records all test data. The pictures of engine-dynamometer and DOC are presented in Photos 1 and 2. The test cell has a full emissions bench with HORIBA MEXA-9100 DEGR analyzer. In this equipment, the CO and CO₂ instruments use the non-dispersive infrared detectors, the NO_x analyzer uses the chemiluminescence principle, the HC analyzer uses the HFID (heating flame ionization detection) method, and the O₂ instrument uses the paramagnetic detector. To measure the NO and NO₂ separately, another analyzer, which ranges from 0 to 2000 ppm with a ± 1 % accuracy of full scale, is utilized.

In order to cover a wide range of temperatures and space velocities representative of engine operations, measurements were conducted at the following steady-state conditions for the three different engine speeds: 9 different temperature points in 1000 rpm, 6 points in 1500 rpm, and 7 points in 1500 rpm. Particularly in low engine speed (1000 rpm), we measured

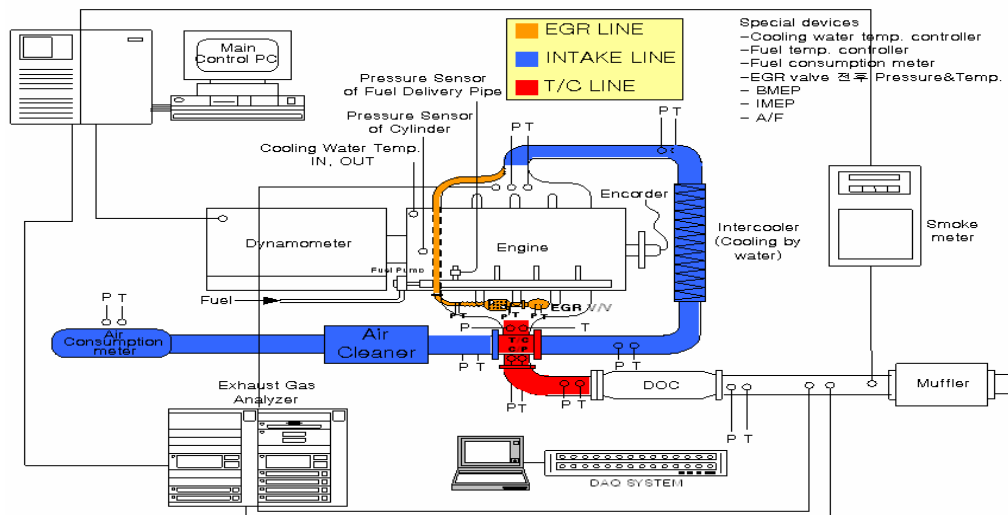


Fig. 1 Schematic view of the experimental set-up

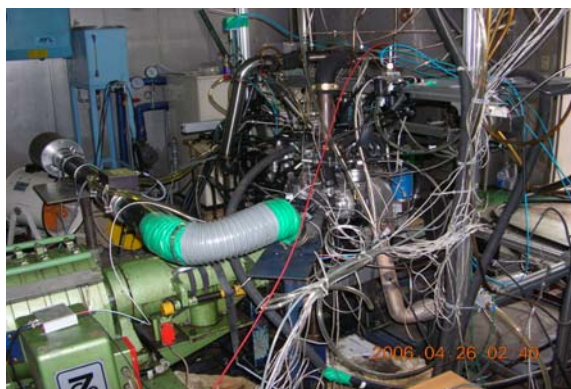


Photo. 1 Picture of engine-dynamometer

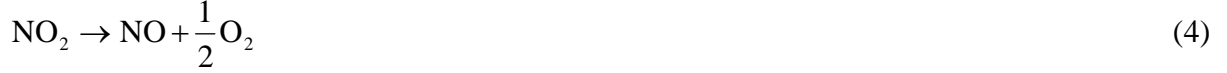


Photo. 2 Picture of DOC

low temperature data to closely evaluate the DOC performance in the vicinity of the light-off. At each fixed engine speed condition, we raised the load to get the successive data with a uniform gap of catalyst temperature. To gain the gas temperatures at inlet and outlet of the DOC monolith reactor, the k-type thermocouples are used. For measuring the catalyst temperatures, we drilled and inserted the thermocouple into the DOC substrate. Here, we assume that the temperature measured at the upper monolith centerline represents all substrate temperatures, because there may be a small temperature difference in it after the DOC reaches its steady-state. To verify if the thermocouple is exactly positioned into the substrate, we checked the concurrent variations of gas and catalyst temperatures and confirmed reasonable separate tendencies.

DOC MODEL

To model the DOC, four reactions are considered. Particularly in this study, since NO_2 as well as NO variation is a matter of concern, NO_2 dissociation is taken into account [1-2]. General carbon number of diesel exhaust hydrocarbons lies between 1 and 40, and is centered in the 9 to 12 range. However, because diesel exhaust has low HC contents in it, selecting the C_9 to C_{12} range of HC as a representative for the total HC would result in low HC concentration levels and make it difficult to model. Thus, the propylene, which has relatively small carbon number, was chosen as a representative HC in this model [3].



For the kinetics of the above reactions, Langmuir-Hinshelwood rate expressions are taken as follows. In the reaction rates, the competition to occupy a catalytic active site between adsorbed-phase species is considered as an inhibition factor.

$$R_{CO} = \frac{k_1 X_{s,CO} X_{s,O_2}}{G} \quad (5)$$

$$R_{C_3H_6} = \frac{k_2 X_{s,C_3H_6} X_{s,O_2}}{G} \quad (6)$$

$$R_{NO} = \frac{k_3 X_{s,NO} X_{s,O_2}}{G} \quad (7)$$

$$R_{NO_2} = \frac{k_4 X_{s,NO_2}}{G} \quad (8)$$

$$G(X_s, T_s) = T_s (1 + K_1 X_{s,CO} + K_2 X_{s,C_3H_6})^2 (1 + K_3 X_{s,CO}^2 X_{s,C_3H_6}^2) (1 + K_4 X_{s,NO}^{0.7}) \quad (9)$$

The adsorption equilibrium constants shown in the inhibition factor can be formulated as the following Arrhenius form. The parameters used are taken from the literatures [4-5].

$$K_i = K_i^o \exp\left(-\frac{E_{a,i}}{R_u T_s}\right), \quad i = CO, HC, NO, NO_2 \quad (10)$$

The reaction rate constants are also formulated as the Arrhenius form, and the parameters are determined through the calibration using the current experimental data. For obtaining the pre-exponential factors and activation energies, which show the best fit, the least square mean method was utilized.

$$k_i = k_i^o \exp\left(-\frac{E_i}{R_u T_s}\right), \quad i = CO, HC, NO, NO_2 \quad (11)$$

Solid-phase mass balance equations for CO, HC, NO, and NO₂ are written as follows.

$$(1 - \varepsilon) \frac{\partial X_{s,i}}{\partial t} = k_{m,i} a_{sf} (X_{g,i} - X_{s,i}) - \frac{a_c R_i}{C_{tot}}, \quad i = CO, HC \quad (12)$$

$$(1 - \varepsilon) \frac{\partial X_{s,NO}}{\partial t} = k_{m,NO} a_{sf} (X_{g,NO} - X_{s,NO}) - \frac{a_c R_{NO}}{C_{tot}} + \frac{a_c R_{NO_2}}{C_{tot}} \quad (13)$$

$$(1 - \varepsilon) \frac{\partial X_{s,NO_2}}{\partial t} = k_{m,NO_2} a_{sf} (X_{g,NO_2} - X_{s,NO_2}) - \frac{a_c R_{NO_2}}{C_{tot}} + \frac{a_c R_{NO}}{C_{tot}} \quad (14)$$

Unlike solid-phase mass balances, the reaction rate terms do not appear in gas-phase formulations because gas-phase species do not participate directly in the catalytic reactions. So, all mass balances for gas-phase species can be written as the following single form.

$$\varepsilon \frac{\partial X_{g,i}}{\partial t} = -u_D \frac{\partial X_{g,i}}{\partial x} - k_{m,i} a_{sf} (X_{g,i} - X_{s,i}), \quad i = CO, HC, NO, NO_2 \quad (15)$$

Solid-phase energy balances are presented in 2-dimensional axisymmetric domains. Here, the heat of reactions is calculated from the enthalpy of formation of each species.

$$(1-\varepsilon)\rho_s c_{p,s} \frac{\partial T_s}{\partial t} = (1-\varepsilon)k_x \frac{\partial^2 T_s}{\partial x^2} + (1-\varepsilon)k_r \frac{1}{r} \frac{\partial}{\partial r} \left(r \frac{\partial T_s}{\partial r} \right) - h_{sf} a_{sf} (T_s - T_g) + a_c n_{sat} \sum (-\Delta H_i) R_i \quad (16)$$

Gas-phase energy balance is

$$\varepsilon \rho_g \frac{\partial (c_{p,g} T_g)}{\partial t} = -\rho_g u_D \frac{\partial (c_{p,g} T_g)}{\partial x} + h_{sf} a_{sf} (T_s - T_g) \quad (17)$$

Catalytic surface area is a critical parameter determining the converter performance. In this study, the catalytic surface area per unit volume of reactor is calculated from the following relations with the properties of Pt/Al₂O₃ [6-7].

$$a_c = S_{Pt} w_{Pt} \quad (18)$$

$$S_{Pt} = \frac{a_{m,Pt} N_A D_{Pt}}{M_{Pt}} \quad (19)$$

SCR MODEL

To model the SCR, three reactions are considered. Although there are many selective DeNO_x reactions in SCR converter, the reaction (21) is assumed as a representative for them. Also, in this study, non-selective ammonia oxidation is taken into the SCR model reactions.



Unlike the DOC model, the SCR kinetics adopts Eley-Rideal mechanism for the DeNO_x and NH₃ oxidation reactions. This means that the gas-phase NO and O₂ react with the solid-phase NH₃. The rate expressions for the above reactions are

$$R_{NO} = \frac{k_{NO} K_{NH_3} C_{NO} C_{NH_3}}{1 + K_{NH_3} C_{NH_3}} - \frac{k_{NH_3} K_{NH_3} C_{NH_3}}{1 + K_{NH_3} C_{NH_3}} \quad (23)$$

$$R_{NH_3} = \frac{k_{NO} K_{NH_3} C_{NO} C_{NH_3}}{1 + K_{NH_3} C_{NH_3}} + \frac{k_{NH_3} K_{NH_3} C_{NH_3}}{1 + K_{NH_3} C_{NH_3}} \quad (24)$$

The NH₃ adsorption equilibrium constants and reaction rate constants are written as follows. Also, the reaction parameters were determined through the SCR experiment, which is not presented in the current paper, and they were used for the simulations.

$$K_{NH_3} = K_{NH_3}^o \exp\left(-\frac{\Delta H_{NH_3}}{R_u T_s}\right) \quad (25)$$

$$k_{NO} = k_{NO}^o \exp\left(-\frac{E_{a,NO}}{R_u T_s}\right) \quad (26)$$

$$k_{NH_3} = k_{NH_3}^o \exp\left(-\frac{E_{a,NH_3}}{R_u T_s}\right) \quad (27)$$

Solid-phase mass balance of NH₃ and gas-phase mass balances of NH₃ and NO are

$$(1-\varepsilon) \frac{\partial C_{s,NH_3}}{\partial t} = k_{m,NH_3} a_{sf} (C_{g,NH_3} - C_{s,NH_3}) - (R_{NO} + R_{NH_3}) \quad (28)$$

$$\varepsilon \frac{\partial C_{g,NH_3}}{\partial t} = -u_D \frac{\partial C_{g,NH_3}}{\partial x} - k_{m,NH_3} a_{sf} (C_{g,NH_3} - C_{s,NH_3}) \quad (29)$$

$$\varepsilon \frac{\partial C_{NO}}{\partial t} = -u_D \frac{\partial C_{NO}}{\partial x} - \left(\frac{3}{2} R_{NO} - R_{NH_3}\right) \quad (30)$$

Since the SCR converter also has the same monolith honeycomb structure, both solid and gas-phase energy balance equations of SCR have the same form as the DOC except in the heat of reaction. The analytic heat and mass transfer coefficients, which are based on the Nusselt and Sherwood numbers obtained from analytical solutions for fully developed laminar flow with constant wall heat flux, are used for the present study as follows [8].

$$k_{m,i} = \frac{Sh_{\infty} D_i}{D_h} \quad (31)$$

$$h_{sf} = \frac{Nu_{\infty} k_g}{D_h} \quad (32)$$

RESULTS AND DISCUSSION

In Fig. 2, the CO, HC, NO, and NO₂ concentrations measured at inlet and outlet of the DOC are plotted against the catalyst temperature at 1000, 1500, and 2000 rpm, respectively. At 1000 rpm, the CO light-off begins at about 160 °C. Also, the DOC exhibits the HC light-off at 190 °C. A complete conversion of CO takes place at temperatures above approximate 180 °C. In the current experiment, the mass transfer limitation effect [3], which the CO downstream concentration slightly increases at higher temperatures due to the higher space velocity, was not observed. Above the light-off, the CO is totally converted, while the HC shows about 65 to 90 % conversion efficiencies. The DOC also shows low (10 to 50 %) conversion performance of NO over a wide temperature range. In particular, at the temperatures below 200 °C, the NO outlet concentration is rather higher than the inlet. This means that, under this operating condition, the NO₂ dissociation is dominant than the NO oxidation. This can be seen from the NO₂ graphs.

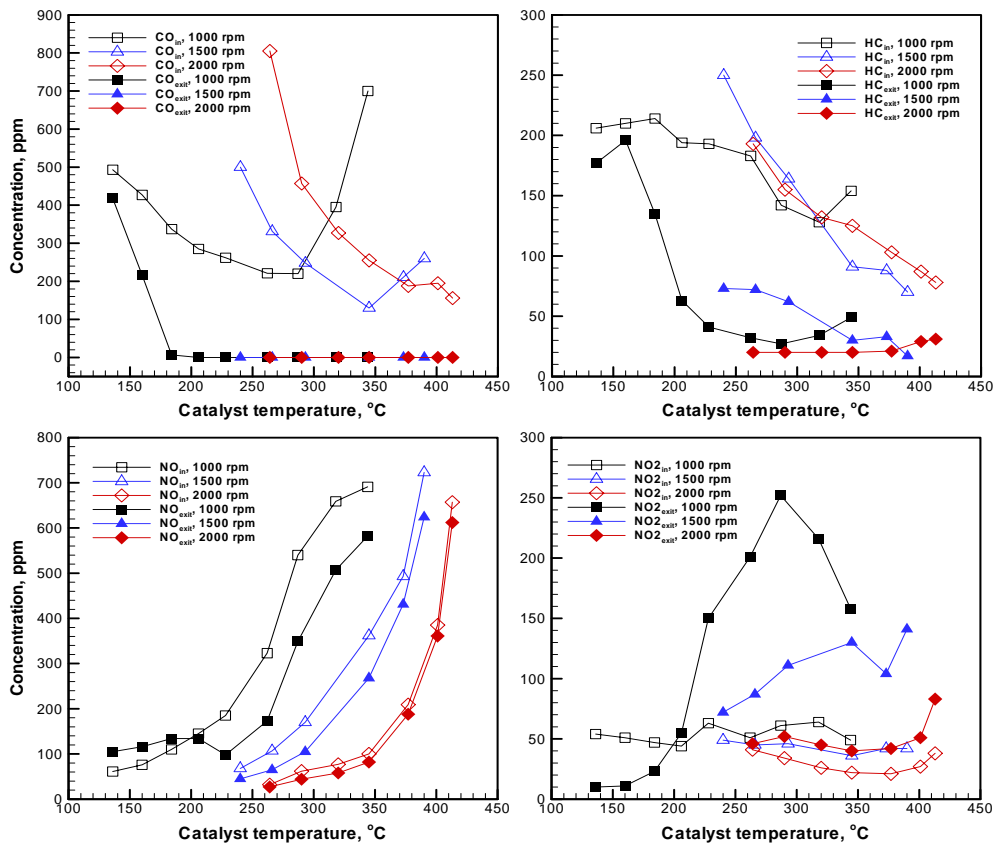


Fig. 2 Concentrations of CO, HC, NO, and NO₂ at inlet and outlet of DOC

In Fig. 3, numerical simulations show the catalyst temperature effect on the CO, HC, NO, and NO₂ conversion efficiencies. As the catalyst temperature increases, the CO and HC present typical light-off behaviors. The CO shows its light-off at 200 °C, and HC 270 °C. At lower temperatures, the NO outlet concentration decreases with increasing the catalyst temperature. However, at temperatures above 270 °C, it goes up because the NO₂ dissociation exceeds the NO oxidation. At higher temperatures, the thermodynamic equilibrium of NO oxidation tends to form an increased fraction of NO [9].

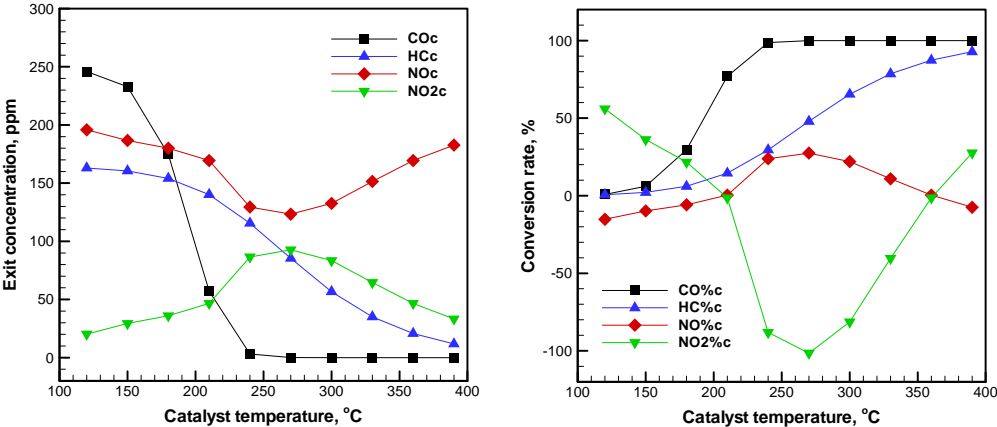


Fig. 3 Catalyst temperature effect on the conversion performance of DOC, operating conditions: CO inlet = 248 ppm, HC inlet = 164 ppmC, NO inlet = 170 ppm, NO₂ inlet = 46 ppm, O₂ inlet = 5.95 %, space velocity = 100000 hr⁻¹

Figure 4 displays the catalyst loading effect on the DOC performance. The actual amount of catalyst loaded on the DOC was set to 100 %, and simulations were conducted with reducing 10 % successively. As the catalyst loading amount becomes smaller, the HC, NO, and NO₂ conversion rates linearly decrease. However, it is interesting to note that the CO conversion rate very slightly decreases. Therefore, regarding only the CO, we can reduce the amount of catalyst loaded on the DOC with a small disadvantage in the conversion.

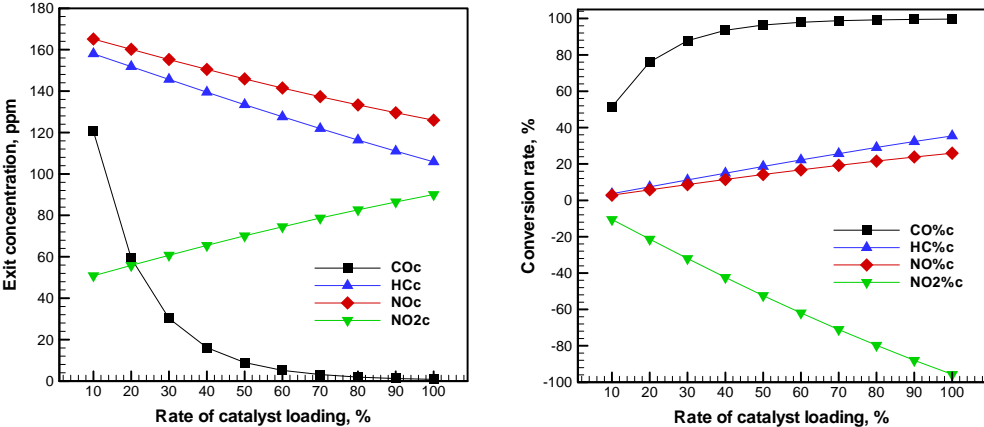


Fig. 4 Catalyst loading effect on the conversion performance of DOC, operating conditions: CO inlet = 248 ppm, HC inlet = 164 ppmC, NO inlet = 170 ppm, NO₂ inlet = 46 ppm, O₂ inlet = 5.95 %, space velocity = 100000 hr⁻¹, catalyst temperature = 300 °C

To see the gas/solid heat exchange behaviour, unsteady simulations were conducted. Figure 5 shows solid temperature distributions within the converter, and all six results are the pictures at 30 sec after the inflow of hot exhaust gas. Three pictures of Fig. 5 (a) present the effect of

space velocity on the gas/solid heat exchange. As the space velocity increases, the heat inflow from the exhaust gas becomes larger so that the temperature of solid substrate, which is initially cold, increases more quickly. Also, three pictures of Fig. 5 (b) display the cell density effect on the heat exchange. As the cell density increases, the converter porosity increases so that the gas/solid heat exchange becomes vigorous.

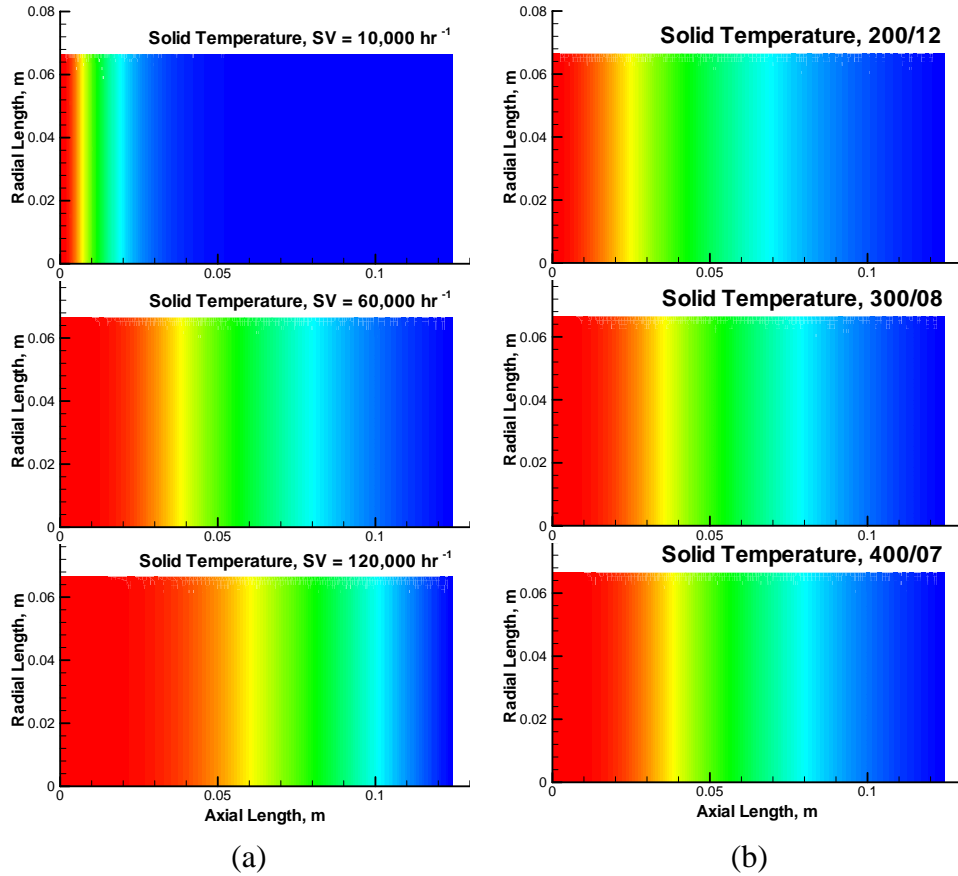


Fig. 5 Solid temperature distributions within the converter (at time = 30 sec), operating conditions of (a): cell density = 400 cpsi, channel wall thickness: 7 m in, inlet gas temperature: 400 °C, initial solid temperature: 20 °C, operating conditions of (b): space velocity = 60000 hr⁻¹, inlet gas temperature: 400 °C, initial solid temperature: 20 °C

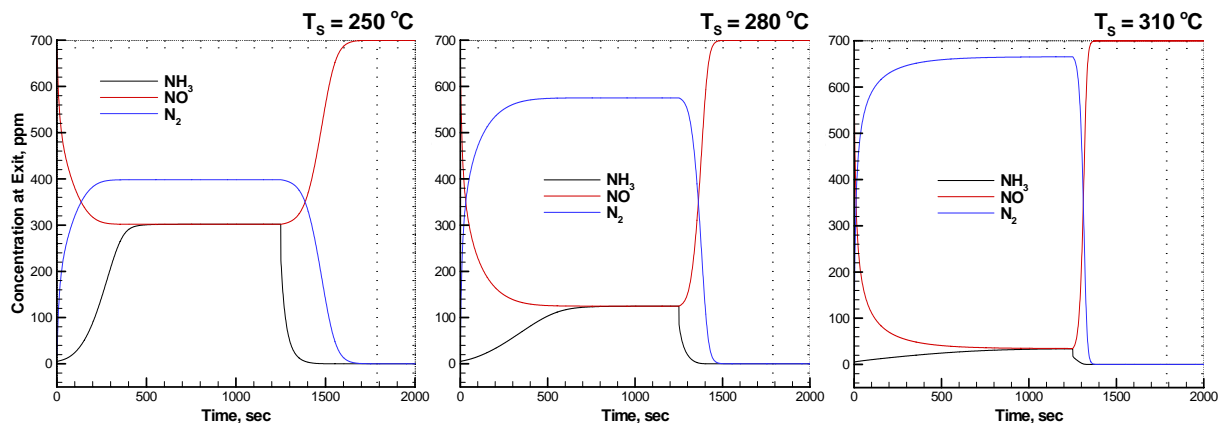


Fig. 6 Transient variation of NH₃, NO, and N₂ over V₂O₅-WO₃/TiO₂ catalyst at different catalyst temperatures, operating conditions: cell density = 400 cpsi, channel wall thickness = 4 m in, space velocity = 100,000 hr⁻¹, NO inlet = 700 ppm (uniform), NH₃ step addition = 700 ppm (0 sec), NH₃ shut-off = 0 ppm (1250 sec)

Figure 6 shows transient DeNO_x performance of SCR, which uses vanadium-based ternary catalyst (V₂O₅-WO₃/TiO₂), at different catalyst temperatures. At the initial periods of all three results, we can see that the NO exit concentration gradually reduces. This is because it takes time for the incoming NH₃ to adsorb onto the catalyst surface and participate in the DeNO_x reaction as an adsorbed-phase. After 1250 sec, due to the NH₃ shut-off, the NO outlet concentration increases up to 700 ppm. However, although there is no NH₃ input as soon as the shut-off, we can observe the occurrence of the SCR reaction, because the already adsorbed NH₃ is available. This SCR reaction continues until the adsorbed NH₃ is totally consumed. Comparing the three results, it is seen that the NO conversion rate increases with an increase in the catalyst temperature.

The present study is an on-going work, not the completed one. After the development of each model on the DOC, DPF, SCR, and other facilities, such as urea injection system, and inlet/outlet header, we aim at integrating all of them into a whole system to utilize this tool on a designing work as well as a comprehensive understanding of the phenomena.

ACKNOWLEDGEMENTS

This work is part of the project ‘Development of Partial Zero Emission Technology for Future Vehicle’ and we are grateful for its financial support.

REFERENCES

- [1] Kandylas I. P. and Koltsakis G. C., “NO₂-Assisted Regeneration of Diesel Particulate Filters: A Modeling Study”, *Ind. Eng. Chem. Res.*, Vol. 41, pp. 2115-2123, 2002
- [2] Haralampous O. A. and Koltsakis G. C., “Back-Diffusion Modeling of NO₂ in Catalyzed Diesel Particulate Filters”, *Ind. Eng. Chem. Res.* Vol. 43, pp. 875-883, 2004
- [3] Triana A. P., Johnson J. H., Yang S. L., and Baumgard K. J., “An Experimental and Numerical Study of the Performance Characteristics of the Diesel Oxidation Catalyst in a Continuously Regenerating Particulate Filter”, SAE 2003-01-3176, 2003
- [4] Oh S. H., and Cavendish J. C., “Transients of Monolithic Catalytic Converters: Response to Step Changes in Feedstream Temperature as Related to Controlling Automobile Emissions”, *Ind. Eng. Chem. Prod. Res. Dev.*, Vol. 21, pp. 29-37, 1982
- [5] Chen D. K. S., Oh S. H., Bissett E. J., and Ostrom D. L., “A Three-Dimensional Model for the Analysis of Transient Thermal and Conversion Characteristics of Monolithic Catalytic Converters”, SAE 880282, 1988
- [6] Bergeret G. and Gallezot P., “in: Handbook of Heterogeneous Catalysis”, Vol. 4, Wiley, New York, 1997
- [7] Crocoll M., Kureti S., and Weisweiler W, “Mean Field Modeling of NO Oxidation over Pt/Al₂O₃ Catalyst under Oxygen-Rich Conditions”, *J. Catalysis*, Vol. 229, pp. 480-489, 2005
- [8] Siemund S., Leclerc J. P., Schweich D., Prigent M., and Castagna F., “Three-Way Monolithic Converter: Simulations versus Experiments,” *Chem. Eng. Sci.*, Vol. 51, No. 15, pp. 3709-3720, 1996
- [9] Madia G., Koebel M., Elsener M., and Wokaun A., “Side Reactions in the Selective Catalytic Reduction of NO_x with Various NO₂ Fractions”, *Ind. Eng. Chem. Res.*, Vol. 41, pp. 4008-4015, 2002